Prediction of Ideal Permeability of Hydrocarbons through an MFI-Type Zeolite Membrane by a Combined Method Using Molecular Simulation Techniques and Permeation Theory

Ryo Nagumo, Hiromitsu Takaba,* and Shin-ichi Nakao

Department of Chemical System Engineering, The University of Tokyo, 7-3-1 Hongo, Bunkyo-ku, Tokyo 113-8656, Japan

Received: February 17, 2003; In Final Form: September 4, 2003

Permeabilities of hydrocarbons (*n*-alkanes from methane to octane) through an MFI-type silicalite membrane were predicted systematically, using a method based on molecular simulation techniques and permeation theory. This method estimates an ideal permeability that will be observed in perfectly crystallized membranes, in which no grain boundaries or defects in the membrane exist. Comparison of the calculated permeability with experimental results will improve our understanding of the effect of structural defects in membranes on changes in permeability. Calculated permeabilities were independent of the molecular weights of the permeates, and showed a "leveling-off" effect related to the increase of the molecular weight of permeates. The estimated permeabilities were an order of magnitude larger than those previously reported in experimental studies. This inconsistency suggests the existence of a permeation barrier in interfaces of crystalline or grain boundaries, resulting from the discontinuous pore networks of zeolite. In addition, concentration profiles of permeating molecules (CH_4, C_2H_6, C_3H_8, and *n*-C_4H_{10}) inside the silicalite membranes were also predicted; these monotonically decreased from the feed side to the permeate side.

1. Introduction

Zeolite membranes, which consist of a thin layer of zeolite crystals, have recently received much attention because of the potential for using their molecular sieving and preferential adsorption properties for the separation process. MFI-type zeolite membranes, including ZSM-5 and its pure silica type silicalite-1, have been investigated in detail,[1,2] mainly because their micropore size (about 0.55 nm) is almost equal to the kinetic diameter of various hydrocarbons. This feature leads to a strong possibility of using these membranes to separate mixtures that are usually difficult to separate, such as organic isomers.[3,4]

However, reported absolute values related to permeability or selectivity are often inconsistent. This is probably because the performance of zeolite membranes depends on their synthesis conditions, and it is virtually impossible to control their structural properties, such as the intercrystalline structure. Because of these difficulties, ideal permeability and the separation mechanisms on zeolite membranes are still obscure. A method based on a theoretical model is thought to be indispensable for determining the potential of zeolite membranes.

To explain the experimental permeation data, van de Graaf et al.[5] measured the separation factors of silicalite-1 membranes for various hydrocarbon mixtures and applied the Maxwell−Stefan equations formulated by Krishna.[6−8] Van den Broeke et al.[9] also investigated the permeation of binary mixtures through a silicalite-1 membrane and compared the binary and the single-component data. Kapteijn et al.[10] applied the Maxwell−Stefan theory, combined with the ideal adsorbed solution theory,[11] to explain the diffusion behavior of hydrocarbon mixtures in zeolites.

Prediction of membrane performance using molecular simulation techniques has recently become popular because these techniques have a high chance of systematically predicting membrane performance and providing various microscopic insights of the permeation mechanism inside the zeolite micropore.[12−14] Krishna et al.[15] combined the Maxwell−Stefan theory with adsorption isotherms obtained from configurational-bias Monte Carlo (CBMC) simulations[16−19] and demonstrated the potential for a high separation factor for the hydrocarbon isomer mixtures through a silicalite membrane. Furthermore, Krishna et al.[20] successfully explained the extremely high selectivity for the separation of hexane isomers reported by Gump et al.[21]

For a more systematic estimation of gas permeability through zeolite membranes, we recently proposed a combined method using molecular simulation techniques and permeation theory.[22] The method has been applied to the calculation of permeabilities of methane and ethylene in silicalite at 301 K. Calculated permeabilities were more than an order of magnitude larger than the experimental data, but the anisotropic permeabilities were in quantitative agreement with the result obtained from grand canonical ensemble molecular dynamics (GCMD) simulations.[23] Nagumo et al. applied this method to predict the permeabilities of inorganic gases (Ar, He, Ne, N_2, and O_2) at 301 K.[24] The calculated permeability was in qualitative agreement with the experimental data, which indicates the validity of our combined method for predicting permeability. In addition, the computational cost of this method is less than that for GCMD simulations for the prediction of permeability in zeolite membranes, even though the GCMD could provide a significant microscopic picture on permeations.[25,26] Our method can accomplish a more systematic prediction of membrane performance than previous methods using molecular simulations. Because of these advantages, some groups have used a similar method to study gas permeation through zeolite membranes. Sholl et al. calculated single-component permeance of Xe and CF_4 through an $AlPO_4$ membrane[27] and of CH_4 and CF_4 through a silicalite mem-

* Corresponding author.

10.1021/jp034401n CCC: $25.00
Published on Web 12/03/2003

brane.[28] Makrodimitris et al. estimated permeabilities of CO_2 and N_2 through silicalite.[29] Each of these studies reported the validity of this method. Further applications of this method for systematic study of the ideal permeability of various permeating species in zeolite membranes are expected.

In this paper, our method is applied to the systematic estimation of permeabilities of normal alkanes (C1−C8) through single-crystal silicalite membranes. The results for the pressure dependence of permeate fluxes and concentration profiles of permeate species are also presented. On the basis of this systematic study, we discuss the influence of shapes or sizes of permeating molecules on the magnitude of the permeability.

2. Methodology

The methodology detail is presented in our previous reports.[22,24] In this section, we briefly explain the methodology.

The relation between the mutual diffusivity, D, and the thermodynamically corrected diffusivity, D_0, is known as the "Darken equation" and is given by

$$D = D_0 \frac{\partial \ln p}{\partial \ln q} \tag{1}$$

where p is the pressure of adsorbate and q is the amount of adsorption.

The corrected diffusivity is often regarded as equal to the self-diffusivity, D_s. Strictly, however, these values agree well only in the limit of an infinitely dilute adsorbate system. Maginn et al. showed this agreement in the transport of methane in silicalite.[25] However, they did not generalize the relation between D_0 and D_s. In our previous work,[22,24] these two diffusivities were distinguished and derived so that D_0 becomes constant, using Maxwell−Stefan theory.[30] Finally, the corrected diffusivity is independent of the site occupancy and the flux of diffusing species was calculated by applying Fick's first law, given by

$$J = -\lim_{\theta \to 0} D_s(\theta) \frac{\partial \ln p}{\partial \ln q} \frac{\mathrm{d}q}{\mathrm{d}x} \tag{2}$$

where x is the position along the direction of permeation, θ is the site occupancy, and J is the permeate flux of adsorbate molecules. Because the value of dq/dx was obtained by assuming the Langmuir adsorption model, the flux can be formulated as follows, when the permeate pressure is assumed to be 0 kPa:

$$J = \frac{\rho D_{s(\theta=0)} q_m}{\delta} \ln(1 + K_A p_0) \tag{3}$$

where q_m is the saturated amount of adsorption, K_A is the Langmuir adsorption coefficient, p_0 and δ are the feed pressure of a permeate species and membrane thickness, respectively, and ρ is the density of the zeolite membrane. The permeability is described by eq 4:

$$P = \frac{\rho D_{s(\theta=0)} q_m}{p_0} \ln(1 + K_A p_0) \tag{4}$$

The Langmuir adsorption model is sometimes insufficient to describe the adsorption properties of longer chain molecules. In such a case, the dual-site Langmuir model[31,32] can describe the adsorption properties precisely. Permeability when the dual-site Langmuir model is introduced is expressed as

$$P = \frac{\rho D_{s(\theta=0)}}{P_0} \{q_{mA} \ln(1 + k_A p_0) + q_{mB} \ln(1 + k_B p_0)\} \tag{5}$$

In the dual-site Langmuir model, adsorption sites are classified into two types, sites A and B, with the respective saturated adsorbed amounts q_{mA} and q_{mB}. The dual-site Langmuir constants for adsorption at the two sites A and B are described by k_A and k_B. Finally, we can estimate the gas permeability using eq 4 or 5.

Concentration profiles of adsorbate species under the steady state can be estimated using

$$q = \{1 - (1 + K_A p_0)^{(x/\delta)-1}\} q_m \tag{6}$$

The parameters needed in the equations are calculated using molecular simulation techniques. Langmuir parameters were estimated using the grand canonical ensemble Monte Carlo (GCMC) technique or the configurational-bias Monte Carlo (CBMC) technique, and the self-diffusion coefficient was calculated by a molecular dynamics (MD) technique. We carried out our simulations using the Cerius2 program supplied by Accelrys K. K. (Tokyo, Japan).

3. Simulations

An MFI-type silicalite crystal structure was used in our simulations. This is represented by the *Pnma* space group (orthorhombic) with lattice parameters $x = 20.022$ Å, $y = 19.899$ Å, and $z = 13.383$ Å. The simulation unit cell used in this study consisted of 12 ($2 \times 2 \times 3$) silicalite unit cells, containing 1152 silicon and 2304 oxygen atoms. A periodic boundary condition was applied in each direction of the simulation cell. Adsorbate concentration in the MD calculation was set at 24−26 molecules/MD unit cell, and intermolecular interactions between adsorbates were ignored. Nonbonding interactions between adsorbates and the zeolite cell were represented by the van der Waals interaction, for which the cutoff length was fixed at 13.8 Å (shorter than half of the length of the simulation unit cell). Thus, the condition is regarded as the limit of an infinitely dilute system. In addition, this procedure allows the analytical data to be taken from the average of 24−26 times the MD simulations, ensuring statistically reliable data from one MD calculation.

As a set of potential functions and parameters of van der Waals and intramolecular bonding interactions, the model used by Vlugt et al.[19] was introduced in our simulations, except for angle and torsion interactions, for which we applied the Burchart 1.01−DREIDING 2.21 force field. The accuracy of this force field has been confirmed by Suzuki et al. in the case of methane and ethylene permeance through a silicalite.[22]

The zeolite framework was considered to be rigid, to reduce the computational cost. An *NVE* ensemble (number of atoms, volume, and total energy in the unit cell are kept constant) was used in the MD simulations. The initial velocity of each atom was set corresponding to the Boltzmann distribution at 301 K. The average temperatures of all MD calculations were within ±50 K of 301 K. The integrated simulation time per MD step was 1 fs. MD simulations of 300 000 (methane and ethane), 500 000 (propane and butane), and 1 000 000 (from pentane to octane) steps were carried out; these step values correspond to 300, 500, and 1000 ps in real time. From the results of these MD simulations, self-diffusivities of each permeate species were calculated using Einstein's equation.

TABLE 1: Comparison of Calculated Isosteric Heats of Adsorption with Experiment[a]

adsorbate	this study	Nijhuis et al.[35]	Hufton et al.[36]	Zhu et al.[37]
C_3H_8	36.8−44.2	35.4−36.6	40.5	40.9
n-C_4H_{10}	47.4−54.3	42.5−48.9	50.2	53
iso-C_4H_{10}	45.3−48.1	43.8	49.3	47.5

[a] Values are kilojoules per mole.

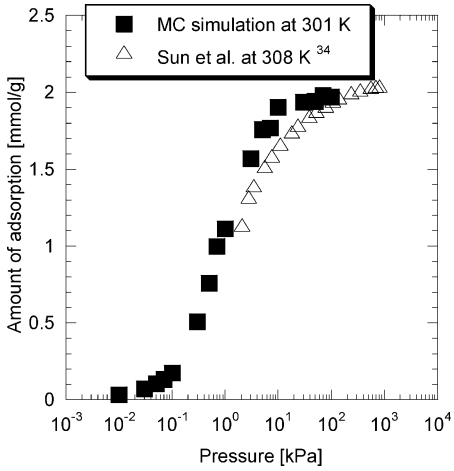

Figure 1. Comparison of calculated adsorption isotherm of propane in silicalite with experimental values.

Introducing the values of self-diffusivity from our MD simulations and adsorption properties from the previous CBMC data[19,33] to permeation theory, we calculated permeabilities and concentration profiles of linear alkanes through silicalite, as discussed below.

4. Results and Discussion

4.1. Adsorption. We estimated permeabilities using sorption data previously reported by Du et al. for CH_4, C_2H_6, and C_3H_8,[33] and Vlugt et al. for n-alkanes from n-C_4H_{10} to n-C_8H_{18}.[19] The force field function of the angle and torsion interactions that we used for MD simulations is not identical to that used by Du et al. and Vlugt et al. Before performing MD simulations, we carried out conventional MC simulations and compared the isosteric heat of adsorption and adsorption isotherms of propane, n-butane, and isobutane with experimental data.[34−37] The calculated isosteric heats and adsorption isotherms on silicalite are presented in Table 1 and Figures 1−3, respectively. For all three species, calculated heats of adsorption and isotherms are in good agreement with those reported in the literature. Thus, our force field is reasonable for describing the adsorption properties and is applicable for MD simulations.

4.2. Dynamics. MD simulations were performed to estimate self-diffusivities of n-alkanes (C1−C8). Generally the self-diffusivity in ZSM-5 has been thought to decrease with an increase in carbon number.[5] As illustrated in Figure 4, however, the isotropic diffusivity that we have estimated by MD calculations is independent of carbon number and shows an unexpected "leveling-off" tendency. To better understand this phenomenon, we analyzed anisotropic self-diffusivities in each direction (Figure 4). The leveling-off trend is found only in the y direction; in the other directions, the self-diffusivities decrease with an increase in carbon number.

This difference between anisotropic diffusivities is attributed to the inherent structure of an MFI-type zeolite. This type of zeolite has two types of pore structure: zigzag channels along the x direction, and straight channels along the y direction.

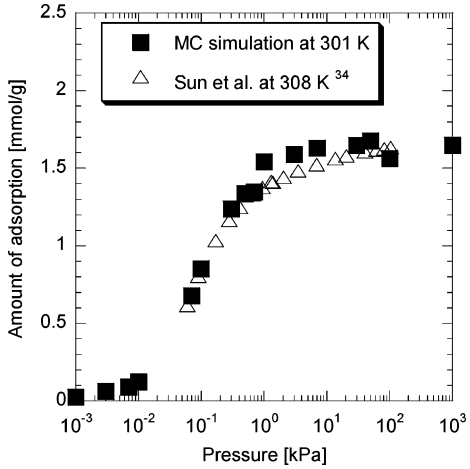

Figure 2. Comparison of calculated adsorption isotherm of n-butane in silicalite with experimental values.

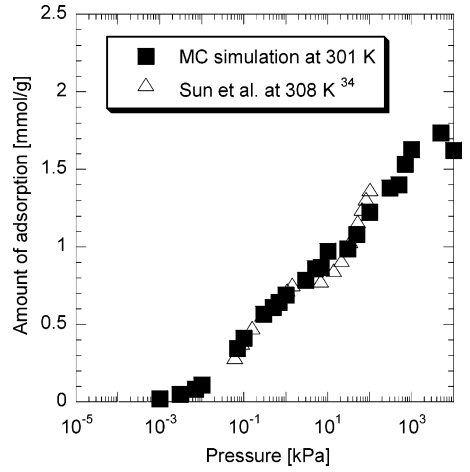

Figure 3. Comparison of calculated adsorption isotherm of isobutane in silicalite with experimental values.

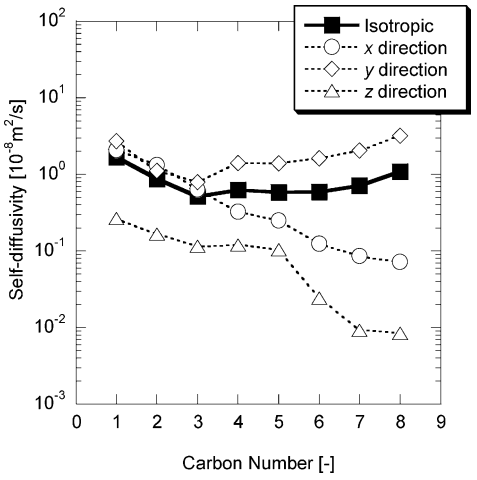

Figure 4. MD calculation results of self-diffusivities for various n-alkanes in silicalite.

Because the pore size is close to the diameter of carbon in n-alkanes, especially in the narrower zigzag channels, the strong interaction between molecules and zeolite pore wall is expected. This interaction would decrease diffusivities along the x and z directions. On the other hand, when molecules are diffusing through larger straight channels, the influence of any interaction with the zeolite framework on diffusion is less than that in the case of diffusion through the zigzag channel, so the diffusivity

TABLE 2: Comparison of Calculated Isotropic Self-Diffusivities for Various *n*-Alkanes with Reported Simulation Results and Experiments[a]

		simulation			NMR	
	this study	MD ref 38	ref 39	MD ref 40	ref 41	ref 42
CH_4	1.7			1.34	1.1	
C_2H_6	0.87				0.54	
C_3H_8	0.51				0.39	0.4
n-C_4H_{10}	0.63	0.461	1	0.17		0.2
n-C_5H_{12}	0.59					0.1
n-C_6H_{14}	0.59	0.304	0.74			0.03
n-C_7H_{16}	0.71	0.371				
n-C_8H_{18}	1.1	0.623	0.76			

[a] Values are $\times 10^{-8}$ m^2/s.

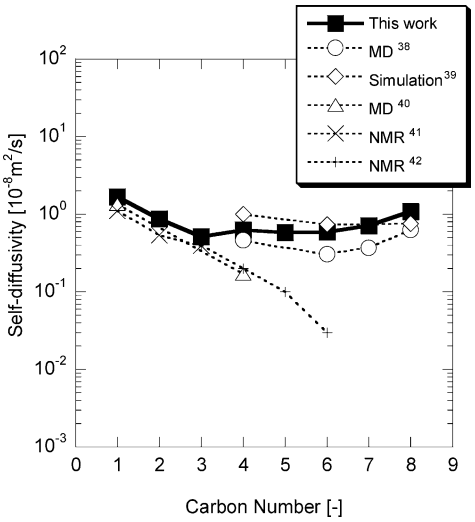

Figure 5. Results of isotropic self-diffusivities of *n*-alkanes in silicalite obtained by different measurement techniques.

does not decrease significantly. In addition, we speculate that the molecular shape is important in determining the diffusion dynamics, because meandering dynamics of linear *n*-alkanes in the straight pore are observed in the graphic analysis of MD results. Thus, the diffusivity along the *y* direction is almost independent of the molecular weight. Consequently, the diffusivity along the *y* direction is so large that it is the predominant contributor to the "average" diffusivity and causes the leveling-off tendency.

To examine the validity of our MD results, a comparison with the reported values obtained from molecular simulations or pulse-field gradient (PFG) NMR is presented in Table 2 and Figure 5. Runnebaum et al.[38] and Maginn et al.[39] obtained simulation results similar to ours. In contrast, Goodbody et al. suggest that an increase in carbon number results in lower diffusivities.[40] It is especially notable that the diffusivities reported by Runnebaum et al.[38] were independent of carbon number, and even for C8, the diffusivity increased compared with that for smaller numbers. They explained this by suggesting a "resonant diffusion mechanism". In this mechanism, the diffusivity reaches its maximum when the chain length of the diffusing molecule is an integral multiple of the length between potential energy barriers. In regard to NMR studies, our MD results for methane, ethane, and propane agree well with reported results.[41,42] For the longer *n*-alkanes, however, the difference in diffusivity between MD and NMR results becomes larger. One possibility for this inconsistency is that the PFG-NMR experiment measured the isotropic diffusivity for methane, ethane, and propane but for longer chained hydrocarbons it measured diffusivity only along the *z* direction. This hypothesis is based on the fact that MFI-type zeolites preferentially grow

TABLE 3: Estimated Isotropic and Anisotropic Permeabilities *P* for Various *n*-Alkanes[a]

	isotropic *P*	anisotropic *P* (*x*/*y*/*z* direction)
CH_4	2.0	2.4/3.2/0.31
C_2H_6	7.3	11/9.3/1.4
C_3H_8	8.1	10/13/1.8
n-C_4H_{10}	13	6.8/30/2.5
n-C_5H_{12}	14	6.2/35/2.6
n-C_6H_{14}	17	3.5/46/0.69
n-C_7H_{16}	21	2.5/60/0.27
n-C_8H_{18}	28	1.8/82/0.21

[a] Values are $\times 10^{-10}$ mol m/(m^2 s Pa).

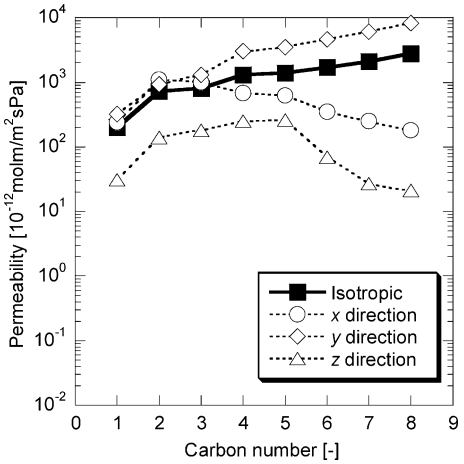

Figure 6. Predicted isotropic and anisotropic permeabilities of *n*-alkanes through silicalite membranes. Feed pressure is assumed to be 101.3 kPa.

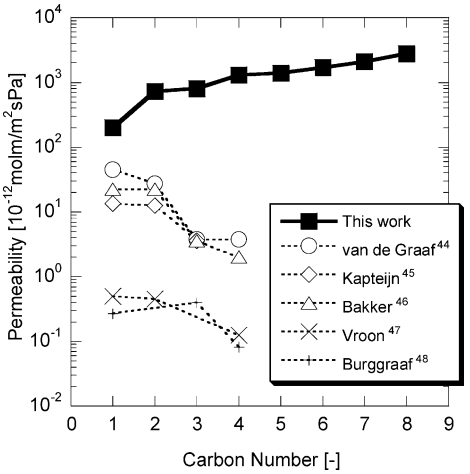

Figure 7. Comparison of predicted permeability for *n*-alkanes in silicalite with experimental values.

in the *z* direction.[43] It should also be noted that the NMR study by Heink et al.[42] measured the diffusivity at 330 K in H-ZSM-5 and not in pure silica zeolite.

4.3. Permeability. Using our MD results and sorption data,[19,33] we estimated permeabilities for C1−C8 *n*-alkanes using eq 4 or 5. Estimated isotropic and anisotropic permeabilities of *n*-alkanes through a silicalite membrane are shown in Table 3 and illustrated in Figure 6. There is a remarkable difference of more than a factor of 10 between the anisotropic permeabilities along the *y* and *z* directions, suggesting that experimental permeabilities depend significantly on the orientation of the zeolite crystals. A comparison with results obtained from previous permeation experiments[44−48] is shown in Figure 7. In this figure, experimental permeabilities decrease with an increase in carbon number. On the other hand, our estimated isotropic

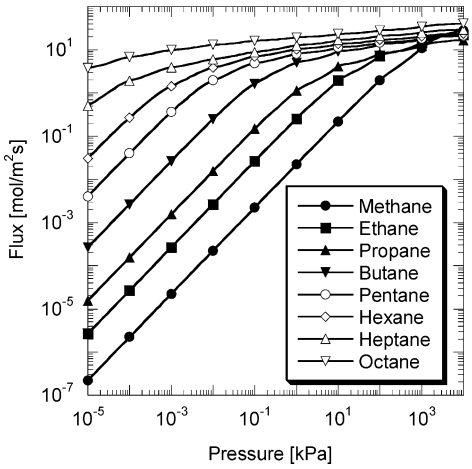

Figure 8. Feed pressure dependence of flux for various *n*-alkanes. Feed pressure is assumed to be 101.3 kPa.

permeability shows a leveling-off tendency and even increases as the number of carbons increases. In addition, calculated values are larger than those previously reported by at least 1 order of magnitude. Some plausible reasons for the difference between our estimated and experimental permeabilities are discussed below.

First, the reason could be attributed to what type of diffusivity is measured by an adopted technique, because eqs 4 and 5 include self-diffusivity for formulation of permeability and not the transport diffusivity. In general, microscopic methods such as PFG-NMR or MD simulations detect the self-diffusivities under equilibrium conditions, whereas macroscopic techniques such as frequency response (FR) or zero-length column (ZLC) can determine transport diffusivities under concentration gradients. Talu et al. calculated diffusivities of *n*-alkanes in the *z* direction from measurement of steady-state flux through a single-crystal membrane.[49] In Figure 8 of that report, they illustrated that microscopic techniques detect larger diffusivities than macroscopic ones. Although our MD data cannot necessarily be compared with those from nonmicroscopic techniques, the data obtained by Talu et al.[49] can be compared with our MD data for the values of self-diffusivities in the *z* direction. Our data become much larger than their values, especially for larger alkanes. Because our method requires the value of self-diffusivities to estimate permeability through a zeolite membrane, it is reasonable that our MD data agree well with the values of self-diffusivities from the microscopic NMR technique (Figure 5).

A second reason for the difference between our estimated and experimental permeabilities relates to the membrane thickness. The membrane thickness in experiments is usually

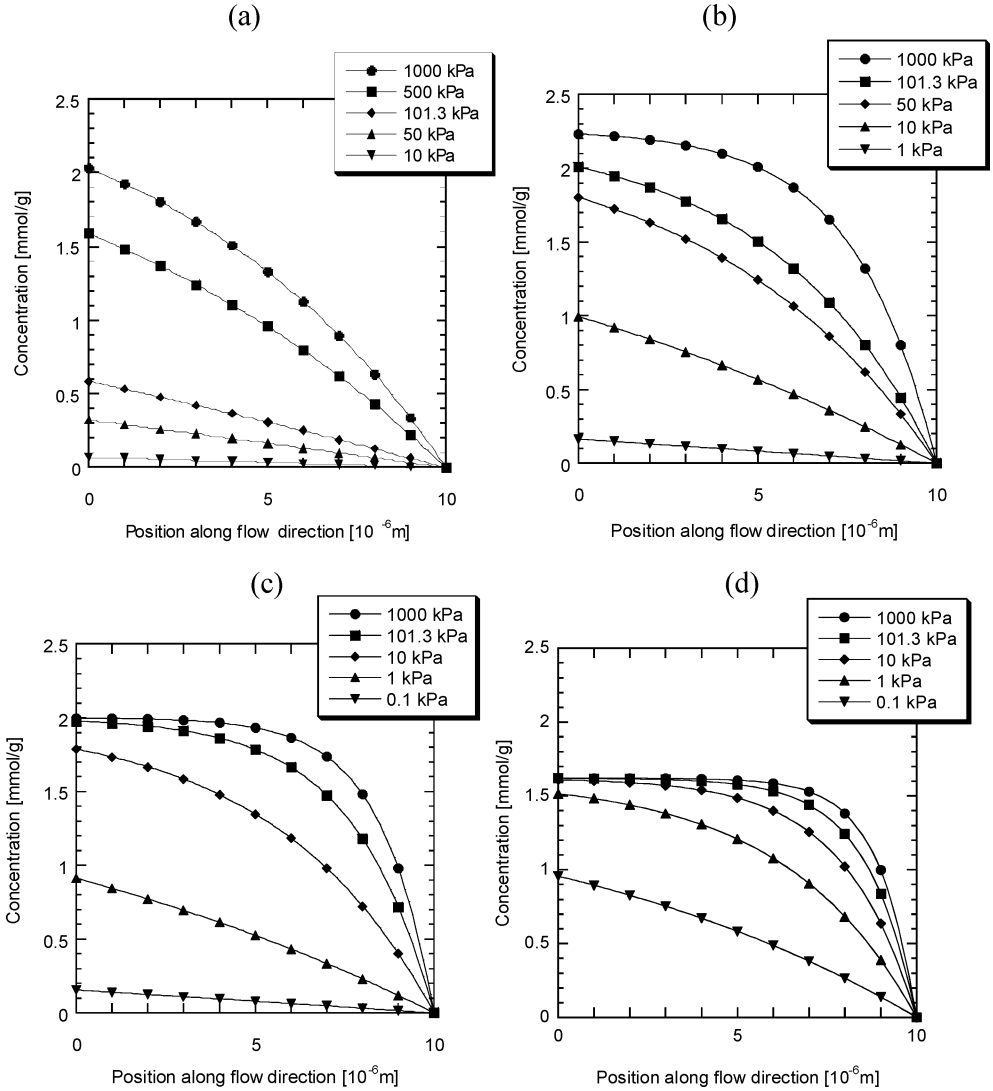

Figure 9. Concentration profiles of permeate in the membranes along the flow direction for (a) methane, (b) ethane, (c) propane, and (d) *n*-butane. Indicated pressure in the plots means the pressure on the feed side.

measured directly from the image of a cross section of a membrane obtained by scanning electron microscopy, but it is difficult to estimate the effective membrane thickness in this way. Because the experimental permeabilities shown in Figure 7 are converted from the reported flux using the membrane thickness obtained from such an optical measurement, there might be an undetermined error.

However, this explanation cannot explain the leveling-off observed for the permeabilities, even if the difference in absolute values can be ascribed to it. To explain the leveling-off trend, it is necessary to consider the differences in zeolite membrane structure between our calculations and experimental conditions. In our method, the model of zeolite membranes is treated as a single crystal with no bare crystalline surfaces. In real zeolite membranes, however, the surface resistance at the entrance and exit of membranes could influence the membrane performance.

To examine such resistance at the entrance side, we analyzed the upstream pressure dependence of the permeate flux of *n*-alkanes, as shown in Figure 8. From this figure, we see that the pressure dependence of the fluxes is not particularly sensitive, especially for larger molecular species. If one supposes that the surface barrier shifts the adsorption equilibrium near the membrane's surfaces, this figure implies that a surface barrier at the upstream side does not contribute significantly to the change of permeability. Ahunbay et al.[50] investigated the diffusion process of methane in the silicalite single-crystal membrane using the GCMD method and concluded that the process is dominated by a barrier during the intracrystalline transport.

However, Ahunbay et al.[50] also noted that surface resistance could become more significant for the permeation of larger molecules through polycrystalline membranes. We consider that Figure 7 reinforces their conclusion because this figure shows that ideal permeability through a single-crystal membrane is much larger than experimental values, especially for larger alkanes. In the case of permeation using a real polycrystalline membrane with several interfaces or grain boundaries inside the microporous network, the contribution of the interface resistances would be cumulative and would be highly likely to act as a barrier to permeation.

Recently, other groups have presented results that support this idea of "interface resistance". Skoulidas et al. used equilibrium MD simulations to examine the kinetic selectivity for several molecular species, such as ethane, *n*-butane, and *n*-hexane, when they enter the mouth of the micropore.[51] According to their investigation, as the carbon chain becomes longer, fewer molecules are able to enter the mouths. They concluded that transport through microporous crystals would be influenced by steric selectivity at the pore mouth. Moreover, Vasenkov et al.[52] investigated the intracrystalline diffusion of methane and *n*-butane molecules by PFG-NMR techniques and suggested the existence of transport barriers within MFI-type zeolite crystals. Martin et al. studied the diffusion of methane through silicalite membranes oriented along the straight channels.[53] Their results showed a strong resistance for flux at both the upstream and downstream surface.

To systemize or theorize the contribution of microscopic resistances at the interfaces or grain boundaries to membrane transportation, further studies are necessary. We are now trying to detect such resistance by experimental methods.

4.4. Concentration Profile. By applying the MC data[33] to eq 6, we calculated the concentration profiles for methane, ethane, propane, and *n*-butane through silicalite membranes (Figure 9a−d). The concentrations decrease monotonically from the upstream side to the downstream, and all of the concentration curves are convex to the top. We note that microscopic information, such as a concentration profile inside the zeolite membranes, can be obtained readily by our method, and this will be useful for the design of a module in engineering applications.

5. Conclusion

Permeability of *n*-alkanes (C1−C8) through a silicalite membrane was predicted systematically using a method based on molecular simulation techniques and permeation theory. Permeability estimated by this method is expected to be an ideal value for a perfectly crystallized membrane with no grain boundaries or defects. Thus, we expect that the contributions of structural discontinuities to the membrane performance can be analyzed by comparing our calculated permeability with the data obtained from permeation experiments.

Our calculated permeability increases with an increase in the molecular weight of the permeate species and becomes larger by an order of magnitude than those reported in the experimental studies. These results suggest the existence of a permeate resistance, resulting from permeation through interfaces and grain boundaries between discontinuous networks of zeolite pores. Further theoretical analysis of the influence of the interface resistance is needed to establish the permeation theory of zeolite membranes and to promote more extensive applications for them, such as the separation of mixtures of large molecular species.

References and Notes

(1) Caro, J.; Noack, M.; Kolsch, P.; Schafer, R. *Microporous Mesoporous Mater.* **2000**, *38*, 3−24.
(2) Lin, Y. S.; Kumakiri, I.; Nair, B. N.; Alsyouri, H. *Sep. Purif. Methods* **2002**, *42*, 229−379.
(3) Sakai, H.; Tomita, T.; Takahashi, T. *Sep. Purif. Technol.* **2001**, *25*, 297−306.
(4) Xomeritakis, G.; Lai, Z. P.; Tsapatsis, M. *Ind. Eng. Chem. Res.* **2001**, *40*, 544−552.
(5) van de Graaf, J. M.; Kapteijn, F.; Moulijn, J. A. *AIChE J.* **1999**, *45*, 497−511.
(6) Krishna, R. *Chem. Eng. Sci.* **1990**, *45*, 1779−1791.
(7) Krishna, R. *Chem. Eng. Sci.* **1993**, *48*, 845−861.
(8) Krishna, R.; Wesselingh, J. A. *Chem. Eng. Sci.* **1997**, *52*, 861−911.
(9) van den Broeke, L. J. P.; Bakker, W. J. W.; Kapteijn, F.; Moulijn, J. A. *AIChE J.* **1999**, *45*, 976−985.
(10) Kapteijn, F.; Moulijn, J. A.; Krishna, R. *Chem. Eng. Sci.* **2000**, *55*, 2923−2930.
(11) Myers, A. L.; Prausnitz, J. M. *AIChE J.* **1965**, *11*, 121−127.
(12) Takaba, H.; Mizukami, M.; Kubo, M.; Fahmi, A.; Miyamoto, A. *AIChE J.* **1998**, *44*, 1335−1343.
(13) Takaba, H.; Matsuda, E.; Nair, B. N.; Nakao, S. *J. Chem. Eng. Jpn.* **2002**, *35*, 1312−1321.
(14) Takaba, H.; Koyama, A.; Nakao, S. *J. Phys. Chem. B* **2000**, *104*, 6353−6359.
(15) Krishna, R.; Vlugt, T. J. H.; Smit, B. *Chem. Eng. Sci.* **1999**, *54*, 1751−1757.
(16) Smit, B.; Siepmann, J. I. *Science* **1994**, *264*, 1118−1120.
(17) Smit, B.; Maesen, T. L. M. *Nature* **1995**, *374*, 42−44.
(18) Bates, S. P.; van Well, W. J. M.; van Santen, R. A.; Smit, B. *J. Am. Chem. Soc.* **1996**, *118*, 6753−6759.
(19) Vlugt, T. J. H.; Krishna, R.; Smit, B. *J. Phys. Chem. B* **1999**, *103*, 1102−1118.
(20) Krishna, R.; Paschek, D. *Ind. Eng. Chem. Res.* **2000**, *39*, 2618−2622.
(21) Gump, C. J.; Noble, R. D.; Falconer, J. L. *Ind. Eng. Chem. Res.* **1999**, *38*, 2775−2781.
(22) Suzuki, S.; Takaba, H.; Yamaguchi, T.; Nakao, S. *J. Phys. Chem. B* **2000**, *104*, 1971−1976.
(23) Pohl, P. I.; Heffelfinger, G. S.; Smith, D. M. *Mol. Phys.* **1996**, *89*, 1725−1731.
(24) Nagumo, R.; Takaba, H.; Nakao, S. *Microporous Mesoporous Mater.* **2001**, *48*, 247−254.
(25) Maginn, E. J.; Bell, A. T.; Theodorou, D. N. *J. Phys. Chem.* **1993**, *97*, 4173−4181.

(26) Nitta, T.; Furukawa, S. *Mol. Simul.* **2000**, *25*, 197−208.
(27) Sholl, D. S. *Ind. Eng. Chem. Res.* **2000**, *39*, 3737−3746.
(28) Bowen, T. C.; Falconer, J. L.; Noble, R. D.; Skoulidas, A. I.; Sholl, D. S. *Ind. Eng. Chem. Res.* **2002**, *41*, 1641−1650.
(29) Makrodimitris, K.; Papadopoulos, G. K.; Theodorou, D. N. *J. Phys. Chem. B* **2001**, *105*, 777−788.
(30) Kärger, J.; Ruthven, D. M. *Diffusion in Zeolite and Microporous Solids*; Wiley-Interscience: New York, 1992.
(31) Micke, A.; Bülow, M.; Kocirik, M.; Struve, P. *J. Phys. Chem.* **1994**, *98*, 12337−12344.
(32) Krishna, R.; Smit, B.; Vlugt, T. J. H. *J. Phys. Chem. A* **1998**, *102*, 7727−7730.
(33) Du, Z.; Manos, G.; Vlugt, T. J. H.; Smit, B. *AIChE J.* **1998**, *44*, 1756−1764.
(34) Sun, M. S.; Shah, D. B.; Xu, H. H.; Talu, O. *J. Phys. Chem. B* **1998**, *102*, 1466−1473.
(35) Nijhuis, T. A.; van den Broeke, L. J. P.; van de Graaf, J. M.; Kapteijn, F.; Makkee, M.; Moulijn, J. A. *Chem. Eng. Sci.* **1997**, *52*, 3401−3404.
(36) Hufton, J. R.; Danner, R. P. *AIChE J.* **1993**, *39*, 954−961.
(37) Zhu, W.; van de Graaf, J. M.; van den Broeke, L. J. P.; Kapteijn, J.; Moulijn, J. A. *Ind. Eng. Chem. Res.* **1998**, *37*, 1934−1942.
(38) Runnebaum, R. C.; Maginn, E. J. *J. Phys. Chem. B* **1997**, *101*, 6394−6408.
(39) Maginn, E. J.; Bell, A. T.; Theodolou, D. N. *J. Phys. Chem.* **1996**, *100*, 7155−7173.
(40) Goodbody, S. J.; Watanabe, K.; MacGowan, D.; Walton, J. P. R. B.; Quirke, N. J. *J. Chem. Soc., Faraday Trans.* **1991**, *87*, 1951−1958.
(41) Caro, J.; Bülow, M.; Schirmer, W.; Karger, J.; Heink, W.; Pfeifer, H. *J. Chem. Soc., Faraday Trans.* **1985**, *81*, 2541−2550.
(42) Heink, W.; Karger, J.; Pfeifer, H.; Datema, P.; Nowak, A. K. *J. Chem. Soc., Faraday Trans.* **1992**, *88*, 3505−3509.
(43) Xomeritakis, G.; Gouzinis, A.; Nair, S.; Okubo, T.; He, M. Y.; Overney R. M.; Tsapatsis, M. *Chem. Eng. Sci.* **1999**, *54*, 3451−3531.
(44) van de Graaf, J. M.; Kapteijn, F.; Moulijn, J. A. *J. Membr. Sci.* **1998**, *144*, 87−104.
(45) Kapteijn, F.; Bakker, W. J. W.; Zheng, G.; Poppe, J.; Moulijn, J. A. *Chem. Eng. J.* **1995**, *57*, 145−153.
(46) Bakker, W. J. W.; van den Broeke, L. J. P.; Kapteijn, F.; Moulijn, J. A. *AIChE J.* **1997**, *43*, 2203−2214.
(47) Vroon, Z. A. E. P.; Keizer, K.; Gilde, M. J.; Verweij, H.; Burggraaf, A. J. *J. Membr. Sci.* **1996**, *113*, 293−300.
(48) Burggraaf, A. J. *J. Membr. Sci.* **1999**, *155*, 45−65.
(49) Talu, O.; Sun, M. S.; Shah, D. B. *AIChE J.* **1998**, *44*, 681−694.
(50) Ahunday, M. G.; Elliott, J. R., Jr.; Talu, O. *J. Phys. Chem. B* **2002**, *106*, 5163−5168.
(51) Skoulidas, A. I.; Sholl, D. S. *J. Chem. Phys.* **2000**, *113*, 4379−4387.
(52) Vasenkov, S.; Bohlmann, W.; Galvosas, P.; Geier, O.; Liu, H.; Karger, J. *J. Phys. Chem. B* **2001**, *105*, 5922−5927.
(53) Martin, M. G.; Thompson, A. P.; Nenoff, T. M. *J. Chem. Phys.* **2001**, *114*, 7174−7181.